

Slab remnants beneath the Baja California peninsula: Seismic constraints and tectonic implications



Hanneke Paulssen*, Denise de Vos

Dept. of Earth Sciences, Utrecht University, Heidelberglaan 2, Utrecht 3584 CS, The Netherlands

ARTICLE INFO

Article history:

Received 21 June 2016

Received in revised form 14 September 2016

Accepted 15 September 2016

Available online 21 September 2016

Keywords:

Gulf of California

Slab

Crust

Mantle

Receiver functions

Surface waves

ABSTRACT

The formation of the Gulf of California has been related to the cessation of subduction of the Guadalupe and Magdalena microplates. Various studies have identified features that point to the presence of a slab remnant beneath the Baja California peninsula, but its depth range and lateral extent remained unclear. In this study we used surface wave phase velocity and receiver function data of NARS-Baja stations around the Gulf of California to better constrain the location of the slab. For stations in central and southern Baja California the shear velocity models show an upper mantle high-velocity layer with its top in the depth range from 115 to 135 km and a thickness varying between roughly 40 and 60 km. These high-velocity anomalies are interpreted as subducted slab remnants. In contrast, the models for the northern peninsula show no slab signature. This change directly correlates with the variation in relative motion between the Baja California peninsula and the Pacific plate as measured by GPS data. It is inferred that the stalled slab fragments beneath the peninsula produce strong coupling between Baja California and the Pacific plate. The shear velocity models for stations on the Mexican mainland show a layer of higher velocities above a low-velocity upper mantle. In the North, the low-velocity mantle, starting at a depth of 40 km, is associated with upwelling as suggested by previous studies. Further south, the transition from higher to lower mantle velocities occurs around 80 km depth, which is a typical value for the lithosphere-asthenosphere boundary. Furthermore, the models show strong crustal thinning towards the gulf, both from the peninsula as well as from the Mexican mainland.

© 2016 The Authors. Published by Elsevier B.V. This is an open access article under the CC BY-NC-ND license (<http://creativecommons.org/licenses/by-nc-nd/4.0/>).

1. Introduction

The Gulf of California forms part of the Pacific - North America plate boundary, linking the San Andreas fault in the North to the East Pacific Rise in the South. The area has a complex tectonic history involving past subduction, followed by a combination of extension, spreading and transform motion. The region evolved after the cessation of subduction of Farallon plate fragments beneath North America around 12.5 Ma, two of which, the Guadalupe and Magdalena microplates, can still be identified offshore of the Baja California peninsula (Lonsdale, 1991, see Fig. 1).

The region has been studied intensively, but a proper understanding of the geodynamical processes that shaped the Gulf of California and the Baja California peninsula is still lacking, partly because the role of the subducted slab fragments and their behaviour in the mantle is unclear. Slab break-off has likely played an important role in the geodynamics and volcanism of the peninsula and gulf

(Castillo, 2008; Ferrari, 2004; Fletcher et al., 2007; McCrory et al., 2009; Michaud et al., 2006; Pallares et al., 2007), but the actual locations of the slab and slab tear are not well constrained. Similarly, the location of a slab window beneath the northern part of the peninsula, inferred from plate reconstructions and volcanism (Atwater, 1989; Dickinson, 1997), is only poorly imaged by seismic studies to date.

Most of the seismic studies that imaged the mantle structure used surface wave data from the NARS-Baja network (Trampert et al., 2003). They have inferred localized low-velocity anomalies in the upper mantle (50–90 km) below the gulf and high velocities below the central to southern part of the Baja California peninsula (Di Luccio et al., 2014; Wang et al., 2009, 2013; Zhang et al., 2009; Zhang and Paulssen, 2012). The high velocities are interpreted as slab remnants beneath the peninsula. However, the lateral and depth extent of these high-velocity anomalies varies between the studies indicating that the location of the slab is not well constrained. The various surface wave studies, for instance, image the top of the slab between 50 and 120 km. Two receiver function studies interpreted this slab interface even much shallower, at approximately 40 km depth, for a station in central Baja California (Obrebski and Castro, 2008; Persaud et al., 2007).

* Corresponding author.

E-mail address: h.paulssen@uu.nl (H. Paulssen).

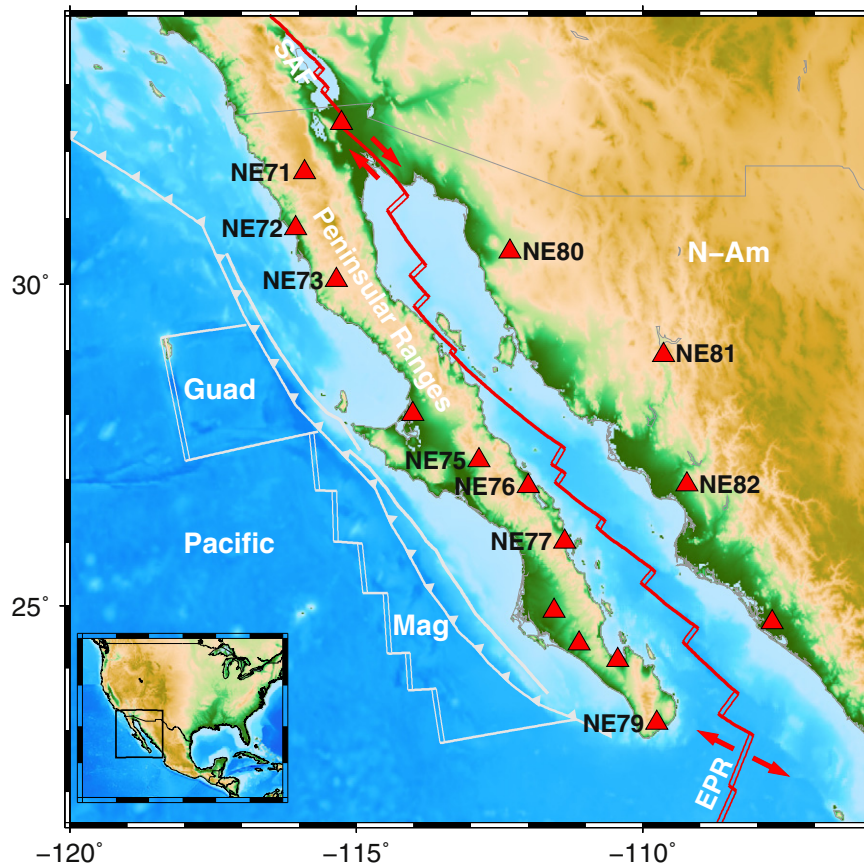


Fig. 1. Map of the Gulf of California region. The current plate boundary is indicated in red, with SAF=San Andreas Fault and EPR=East Pacific Rise. White lines represent ancient plate boundaries, as obtained from Lonsdale (1991). N-Am=North-American plate; Pacific=Pacific plate; Guad=Guadalupe microplate; Mag=Magdalena microplate. Triangles indicate locations of the NARS stations. Inversions were performed for stations given with their station codes.

In this study we combine phase velocity data, which constrain the overall shear velocity structure with depth, with receiver function data, that are more sensitive to sharp velocity changes, to better determine the mantle structure beneath the NARS-Baja stations. In addition, our models provide further constraints on variations in the crustal structure around the Gulf of California.

2. Methods and data

Because of their complementary in sensitivity to shear velocity structure, surface wave and receiver function data have often been inverted jointly in studies of crustal and uppermost mantle structure (e.g., Julià et al., 2000; Özalaybey et al., 1997; Shen et al., 2013b). In this study we used newly measured P-wave receiver functions for stations of the NARS-Baja network and combined them with existing Rayleigh wave phase velocity data obtained by Zhang and Paulssen (2012) to invert for crustal and upper mantle shear velocity structure beneath the NARS-Baja stations around the Gulf of California.

2.1. P-wave receiver functions

We used the standard receiver function approach by Langston (1979) to determine the receiver functions of the NARS-Baja stations. A receiver function is obtained by deconvolution of the direct P-wave signal plus its coda recorded on the radial component by that on the vertical component. This effectively eliminates the source time

function and makes the receiver function mainly sensitive to P-to-S converted waves at the receiver side of the ray path. The receiver function is filtered in the frequency domain by a Gaussian filter of width a and a waterlevel parameter c to stabilize the deconvolution (Langston, 1979). For our study we used $a = 2$ and $c = 0.001$ to obtain stable, but sufficiently high-frequency receiver functions. The receiver functions were obtained for a 40 s time window after the P arrival to include P-to-S conversions from the upper mantle. We collected data from 893 events at distances between 40° and 90° with a minimum magnitude of 5.5. Seismograms with a poor signal-to-noise (S/N) ratio were discarded as well as unstable receiver functions caused by fluctuations of the horizontal components due to ground tilting. As an example, the individual receiver functions of station NE76 are shown in Fig. 2a. With most of the events at back azimuths around 125° (SE), 240° (SW) and 320° (NW), the data were divided around these three dominant back azimuth directions. For each of these directions, the receiver functions were averaged, mostly over two or three slowness ranges. The benefit of using average receiver functions is that they have an improved S/N ratio compared to the individual receiver functions. The averaging also enables determination of the (time-dependent) standard deviation as a measure of the uncertainty. The different slowness values, or incidence angles of the incident P wave, are important to better constrain the shear velocity structure (Ammon et al., 1990; Paulssen et al., 1993). For 10 stations, indicated by their station codes in Fig. 1, we had sufficient numbers (66 to 252) of receiver functions to determine reliable average receivers functions. The other stations

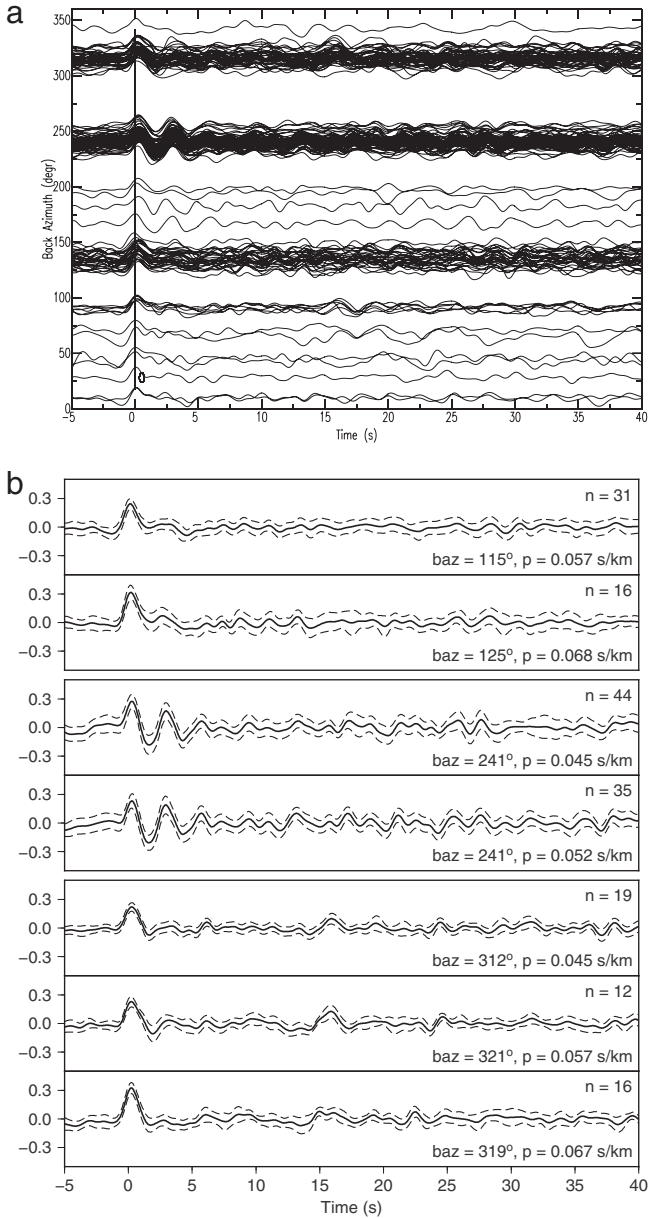


Fig. 2. (a) Individual receiver functions of station NE76 as a function of back azimuth. (b) Average receiver functions (solid) with one standard deviation uncertainty (dashed). The number of receiver functions (n), the average back azimuth (baz), and average slowness (p) are indicated in each panel. The top two receiver functions are for SE, the middle two for SW, and the bottom three for NW back azimuths.

did not have sufficient data, mostly because these stations were not operational for the whole duration of the project. Per station, we obtained up to four average receiver functions with different slowness values for each of the three dominant back-azimuthal directions (SE, SW, NW). Fig. 2b shows the average receiver functions for station NE76 with standard deviation for SE (two receiver functions), SW (two) and NW (three) back azimuths. Clear azimuthal variations are observed, mainly in the first 5 s corresponding to P-to-S conversions from the crust, revealing effects of heterogeneity and/or anisotropy. We will come back to this later.

2.2. Phase velocity data

We used the Rayleigh wave phase velocity data of Zhang and Paulssen (2012) to determine the phase velocity curves at each of

the stations. Their study is based on a data set of 858 earthquakes with a moment magnitude larger than 5. They used the two-station method, first developed by Sato (1955), to determine phase velocities for the paths between stations of the NARS-Baja project. Multiple events have been used to determine an average phase velocity curve for each interstation path. Each curve was obtained as the average of at least 8, but in most cases more than 20, individual phase velocity curves with a minimum of 4 measurements per period. The average phase velocity curves were subsequently inverted for phase velocity maps at multiple periods by linear inversion of the path averaged data for a 100 km spaced grid. The phase velocity curves at the station locations were obtained by interpolation of the three nearest phase velocity curves of the grid using inverse distance weighting (Shepard, 1968). The phase velocity curves were obtained for periods from 10 to at least 160 s, but in most cases to 250 s. The estimated uncertainty for the phase velocity curves is 0.5%, a value adopted from Zhang and Paulssen (2012).

2.3. Joint inversion of receiver function and phase velocity data

The receiver functions and phase velocity data at each of the stations were jointly inverted to determine the crustal and upper mantle structure to a depth of approximately 200 km. Rather than taking a linearized approach (e.g., Julià et al., 2000), we chose to use the Neighbourhood Algorithm (Sambridge, 1999a) to investigate the distribution of models that fit the data within the uncertainty. The Neighbourhood Algorithm is a guided random search method with preferential sampling of the model space in regions of good data fit. It divides the model space in nearest neighbour regions (Voronoi cells) constructed from the distribution of model samples for which the misfit has already been calculated. In the regions of the n_r models with lowest misfit, n_s new models are randomly generated, and the process is repeated. While regions of low misfit are preferentially sampled, the model space can still be fully explored with a proper selection of the tuning parameters n_s , n_r and the number of iterations. The method is therefore suited to assess the distribution of acceptable models. Here we used $n_s = 200$, $n_r = 75$ and 500 iterations. These numbers were selected as the best combination between a wide model search and fast convergence.

The Neighbourhood Algorithm can also be used to estimate the posterior probability density function from the complete set of models using the model appraisal approach of Sambridge (1999b). However, in view of the back-azimuthal variations that we observe in the receiver function data for most of the stations (see Fig. 2, for example) we only interpret the robust features of our models. Calò et al. (2016) used the trans-dimensional Bayesian formalism to determine the crustal and uppermost mantle structure for North American stations. This approach would not be useful for our stations because quantitative error estimates of the 1-D parameters may not be meaningful in case of more complex structure. In Section 3.3 we will return to the issue of crustal deviations to 1-D structure.

Not favouring one type of dataset above the other, we decided to give equal weights to the receiver function and phase velocity data. The misfit is therefore defined as

$$M = 0.5M_{RF} + 0.5M_{PV} \quad (1)$$

where the receiver function misfit is

$$M_{RF} = \frac{1}{N} \sum_{j=1}^N \frac{1}{n} \sum_{i=1}^n \left(\frac{RF_j^{obs}(t_i) - RF_j^{pred}(t_i)}{\sigma_j^{RF}(t_i)} \right)^2 \quad (2)$$

with $RF_j^{obs}(t_i)$ and $RF_j^{pred}(t_i)$ the j th observed (average) and predicted receiver functions as a function of time sample t_i , respectively, and

$\sigma_j^{RF}(t_i)$ the standard deviation of the data. n is the number of samples per receiver function and N the number of receiver functions. Similarly, the phase velocity misfit is

$$M_{PV} = \frac{1}{m} \sum_{i=1}^m \left(\frac{PV^{obs}(T_i) - PV^{pred}(T_i)}{\sigma^{PV}(T_i)} \right)^2 \quad (3)$$

with $PV^{obs}(T_i)$ and $PV^{pred}(T_i)$ the observed and predicted phase velocity data as a function of period T_i , respectively, and $\sigma^{PV}(T_i)$ the uncertainty of the data. m is the number of periods of the phase velocity curve.

The predicted receiver functions were calculated by the Thomson-Haskell method for 1-D models consisting of six layers. The first three layers comprise the crust (sediments, upper and lower crust) and the lower three the mantle structure. The model parameters are shear velocity (v_s), P-to-S velocity ratio (v_p/v_s), and layer thickness (h), which vary within the ranges shown in Table 1. The density was scaled to the P-wave velocity according to the empirical relation given by Brocher (2005). Fig. 3 shows the allowed range of shear velocity models with an example input model. The phase velocity curves were calculated for the model that was linearly extrapolated to reference model MC35 (van der Lee and Nolet, 1997) at 420 km and similar at greater depths. The program *rayleigh* (courtesy G. Nolet) was used to calculate the phase velocity curves.

The main goal of the inversion approach was not to find the model that best fits the data, but rather to investigate the consistent features of the best fitting models to determine the robust features of the most likely models.

3. Results

3.1. Results for station NE76

The inversion approach is first illustrated for station NE76. The Neighbourhood Algorithm was applied to the phase velocity curve of this station and the (average) receiver functions from all back-azimuth directions. The results are shown in Fig. 4a as a model density plot of all models that fit the data with a misfit less than 1, that is, within the estimated uncertainties. The highly sampled regions of the model space are indicated in blue, the more poorly sampled regions in yellow. The grey regions only contain models with a misfit larger than 1. Out of the 100,200 investigated models, 61,349 models fit the data with a misfit smaller than 1. Although this implies that each of these models fits the data within the uncertainty, we can infer the more likely structure from the density distribution of the models because the Neighbourhood Algorithm preferentially searches in regions of lowest misfit. The best fitting models, represented by the highest model density, are clustered around the model with the smallest misfit represented by the red line. The average of all the sampled models is shown by the white line. Its similarity to the best model indicates a model distribution around this best model and convergence towards this model. In the crust, velocity jumps

Table 1
Model parameterisation with allowed ranges for v_s , v_p/v_s , and layer thickness h .

Layer	v_s (km/s)		v_p/v_s		h (km)	
	min	max	min	max	min	max
1	1.5	3.0	2.00	3.00	0	5
2	2.6	3.8	1.65	1.85	5	20
3	3.2	4.3	1.65	1.85	5	20
4	3.7	4.9	1.65	1.85	10	100
5	3.7	4.9	1.65	1.85	20	70
6	3.7	5.3	1.65	1.85	–	–

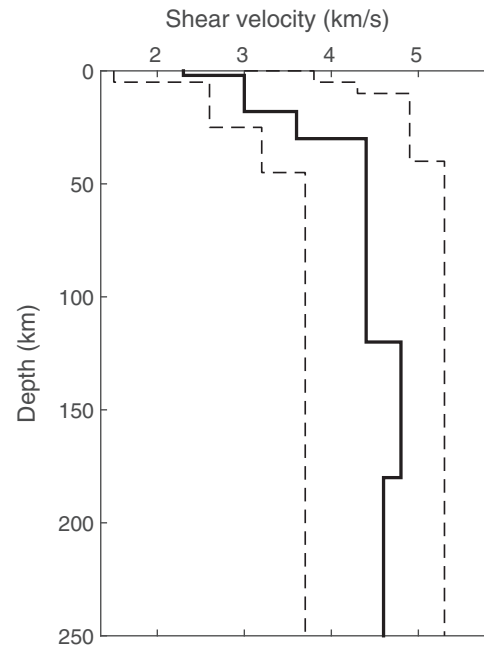


Fig. 3. Boundaries of potential shear velocity models (dashed lines). An example input model is shown by the solid line.

around 4 and 22 km depth indicate the base of the sediment layer and Moho depth, respectively. In the mantle, a high-velocity region is found between depths of approximately 130–140 and 190–200 km.

The fits of the best model to the receiver functions and phase velocity data are shown in Fig. 4b and c, respectively. The velocity jump at 4 km causes the broadening of the first peak in the receiver functions by interference of the direct P wave with the P-to-S conversion from the base of the sediment layer. The receiver function peak at 3 s is produced by the P-to-S conversion from the Moho. The positive peak around 15 s and the negative peak at 21 s are caused by conversions from the velocity increase and decrease at around 140 and 200 km depth, respectively. The best model has a misfit of 0.53, with a receiver function misfit of 0.56 and phase velocity misfit of 0.51, which each contribute for 50% to the total misfit.

To further investigate the individual dependence on the phase velocity and receiver function data, separate inversions were performed for phase velocity and receiver functions only, with the results shown in Fig. 5a and c, respectively. The models of the phase velocity inversions are more poorly constrained than those of the joint inversion as can be inferred from a less pronounced distribution around the best model and a larger discrepancy between the best model (red) and the average of all models (white). However, the four most prominent velocity jumps around 4, 22, 130 and 190 km can also be recognized in the phase velocity inversions. The low number of models (2441) that fit the receiver function data within the uncertainty as well as the unrealistic velocity distribution with depth is caused by the azimuthal variations of the receiver function data. Yet, the receiver function data independently identify velocity increases at roughly 4, 22 and 130 km depth, indicating that the velocity increases at these depths must be sufficiently sharp to generate converted phases. There is no evidence for a sharp velocity decrease around 190–200 km depth based on the receiver function data.

3.2. Results - mantle structure

The procedure illustrated for station NE76 was also used to determine the structure for the other stations. Fig. 6 shows the joint

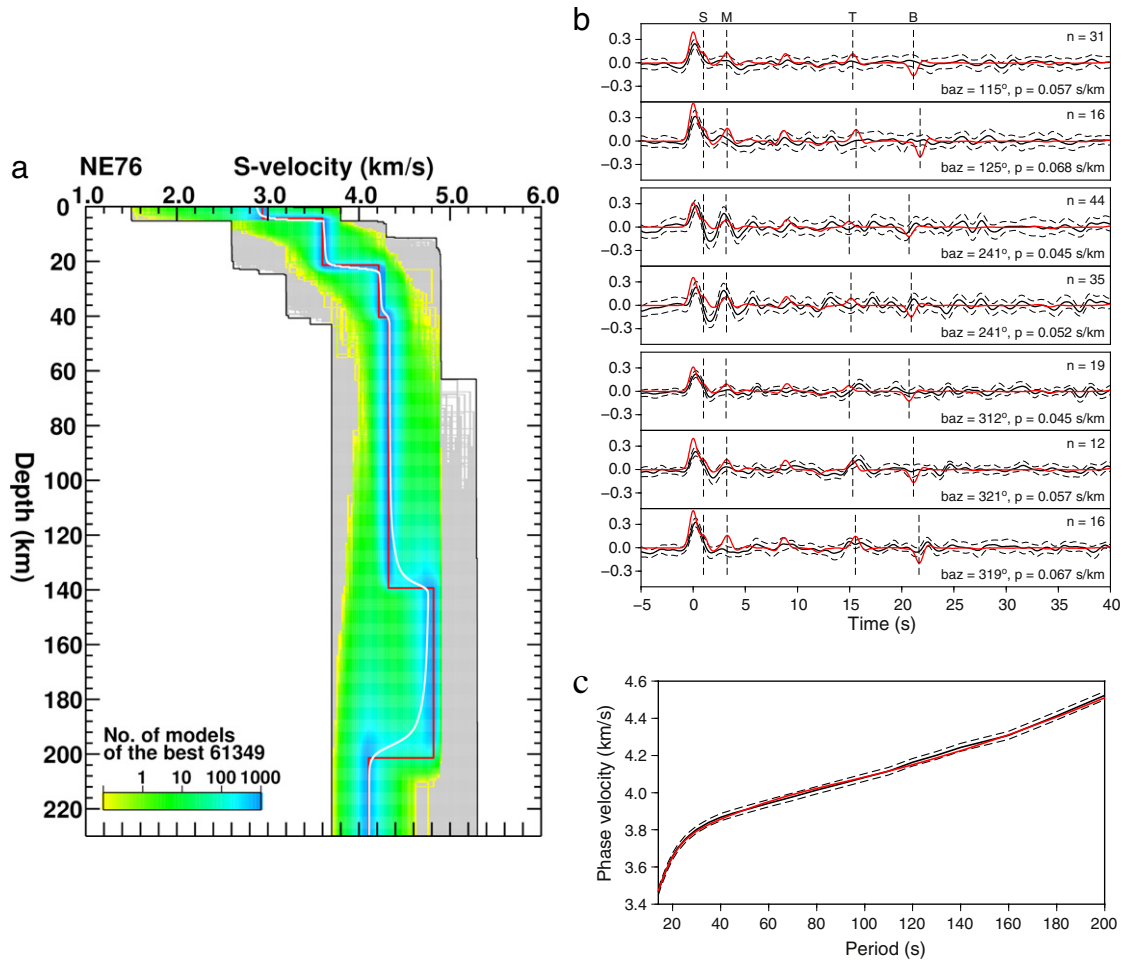


Fig. 4. (a) Model distribution for the joint inversion for station NE76. Black lines delineate the boundaries of the model space search and grey areas indicate regions of the model space containing models with a misfit larger than 1. Yellow to blue areas indicate regions with models with a misfit smaller than 1. The white line represents the average of all models and the red line the lowest misfit model. (b) Observed (black) and best-model synthetic (red) receiver functions with 1 standard deviation uncertainty (dashed). P-to-S conversions from the base of the sedimentary layer (S), Moho (M), top (T) and bottom (B) of the high-velocity anomaly are indicated by dashed bars. (c) Observed (black) and best-model (red) phase velocity curves with 0.5% uncertainty (dashed).

inversion results for stations NE73, NE75, NE76, NE77, and NE79 that are located on the Baja California peninsula. Note that the misfit of the best model for station NE73 is larger than 1. The model density plot of this station therefore does not show the models with a misfit smaller than 1, but the distribution of the best 1000 models. The common feature of all the low-misfit models of Fig. 6 is a high-velocity layer in the mantle. For NE73, NE76 and NE77, this layer is approximately 60 km thick, for NE75 and NE79 it is somewhat thinner (40 and 50 km, respectively). The top of this layer is found at depths of roughly 115 km to 135 km. The high-velocity anomaly is obtained from the phase velocity inversions for each of the stations, but is generally more poorly constrained than for the joint inversions. In addition, except for station NE75, the receiver function inversions independently identify a sharp velocity increase around 130 km depth, that is, at the top of the high-velocity anomaly. The velocity increase at the top of the layer is therefore sharper and better constrained than the velocity decrease at the bottom.

In contrast to the results for the other stations on the peninsula, the presence of an upper mantle high-velocity anomaly is not clear in the model distributions of stations NE71 and NE72 in the northern part of the peninsula (see Fig. 7). The low-misfit models only show a small amplitude high-velocity anomaly that is mainly determined

by the phase velocity data. The receiver function inversions show no evidence for velocity increases or decreases at depths corresponding to those of the phase velocity inversions. We therefore conclude that the presence of an upper mantle high-velocity anomaly is not obvious below stations NE71 and NE72.

The upper mantle models for stations NE80, NE81 and NE82, located on the Mexican mainland, are distinct from those on the Baja California peninsula because they show a velocity decrease in the upper 100 km of the mantle (see Fig. 8). The largest gradient of the velocity decrease occurs around 40 km depth below station NE80, whereas it is found at 70 to 100 km for stations NE81 and NE82.

3.3. Results - crustal structure

We determined the most robust features of the crustal structure by inversions using receiver functions only. Phase velocity data, with periods of 10 to 20 s, are sensitive to crustal structure, but there are strong trade-offs between v_s and the depths of discontinuities (Lebedev et al., 2013). In addition, our phase velocity data are interpolated from a 100 km spaced grid, and therefore lack the lateral resolution of the strongly varying crustal structure that has been shown to exist in previous receiver function studies

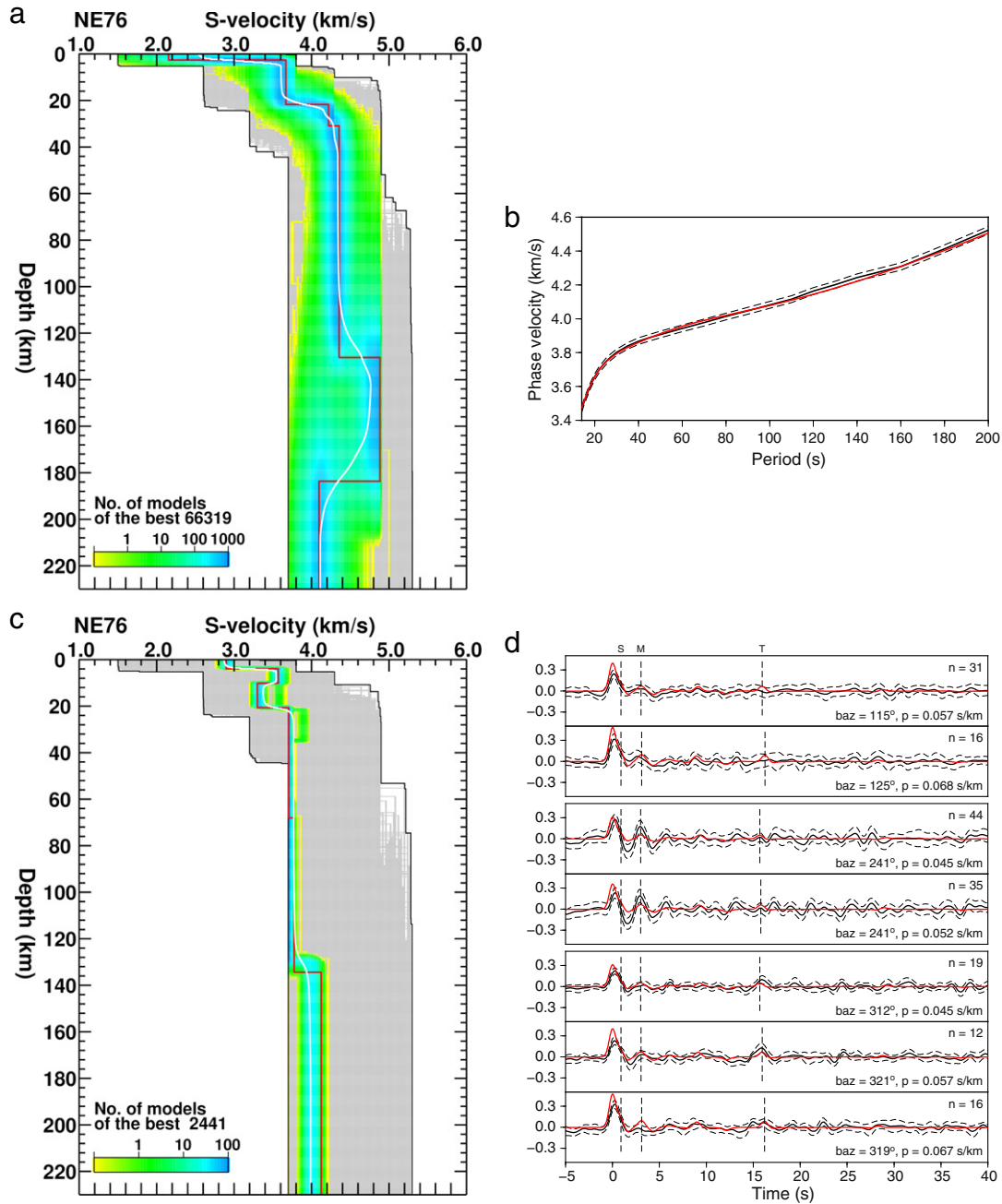


Fig. 5. (a) Model distribution for the phase velocity inversion for station NE76. (b) Observed (black) and best-model (red) phase velocity curves. (c) Model density distribution for the receiver function inversion. (d) Observed (black) and best-model synthetic (red) receiver functions. See Fig. 4 caption for further explanation.

(Lewis et al., 2001; Persaud et al., 2007). The back-azimuthal dependence of the receiver function data (see Fig. 2) provides additional evidence of small-scale crustal heterogeneity. To infer the consistent crustal features per station, we inverted the data from all back azimuths, and for each of the three dominant back-azimuth directions (SE, SW, NW) separately. This allows to identify some of the biases or artefacts caused by 1-D modelling of a more complex structure.

The most prominent and consistent features of the models were the base of the sediment layer and the Moho discontinuity, where the Moho was interpreted as the largest velocity increase between 10 and 40 km depth. Table 2 gives depth ranges obtained for the sediment interface and Moho as inferred from all four inversions per

station. The stations with the largest sediment thicknesses (with values up to 4 or 5 km), but also with the largest sediment thickness variations, are found in coastal regions, i.e. at stations NE72, NE76, NE77, NE79 and NE82. The low elevation of these stations with the large gradients in topography explain these findings.

The inferred Moho depths range from 20 to more than 30 km (see Table 2). Here it should be noted that the receiver function inversions for station NE77 gave poorly constrained Moho depths and large Moho depth variations. To stabilize the results, the depths were determined from inversions that included the phase velocity data as well. The largest crustal thicknesses, with values of more than 30 km, are found for stations NE71, NE72, and NE73, located at the

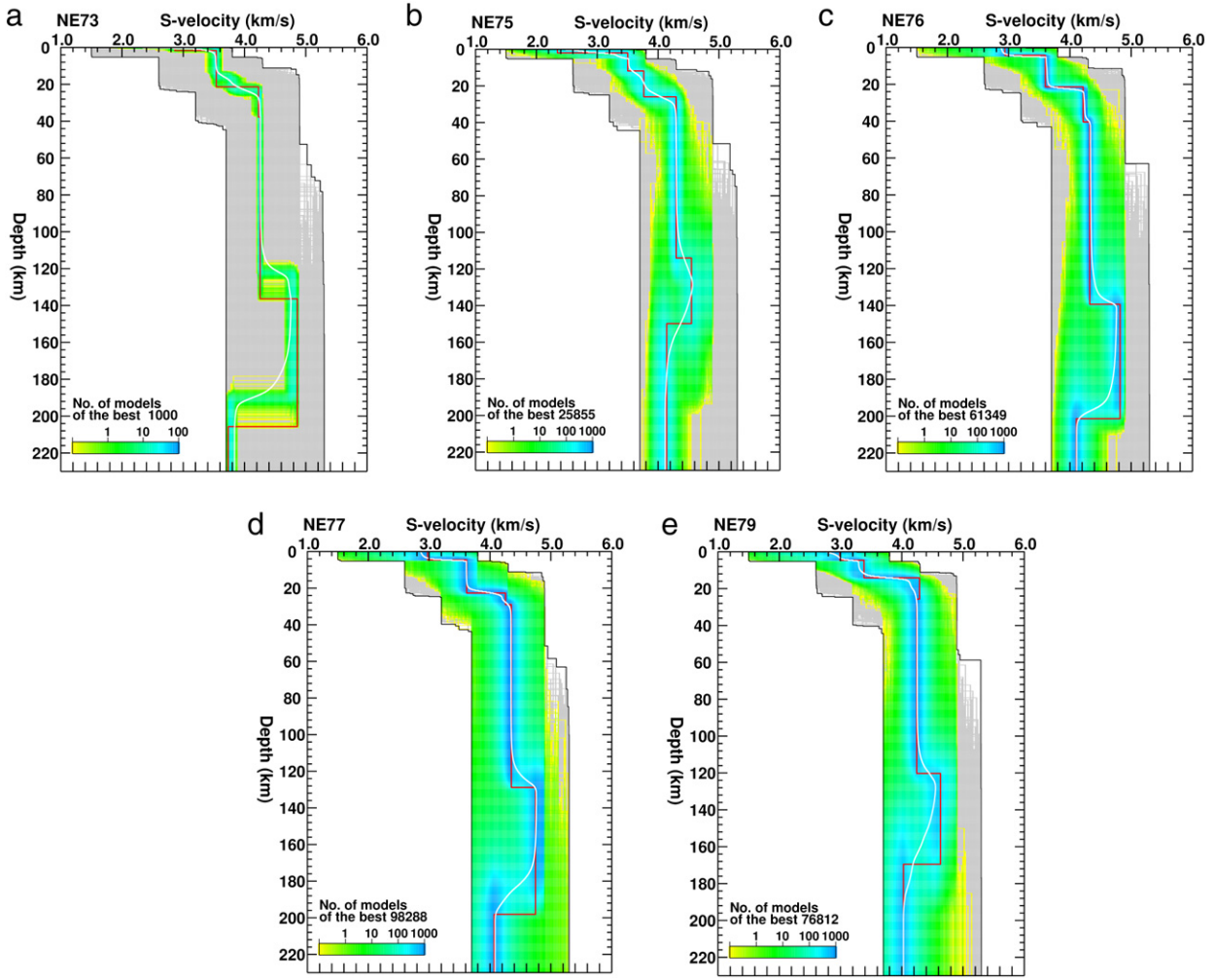


Fig. 6. Model distributions for the joint inversions for station (a) NE73, (b) NE75, (c) NE76, (d) NE77, and (e) NE79. See Fig. 4 caption for further explanation.

western side of the Peninsular Ranges in the northern part of the Baja California peninsula. Shallower Moho depths (19–27 km) are obtained for the central and southern peninsula. Overall, we observe crustal thinning towards the gulf: the crustal thickness of more than

30 km west of the Peninsular Ranges decreases to 19 km at the east coast of the peninsula. At the other side of the gulf, beneath the Mexican mainland, we find Moho depths that increase again from approximately 20 km at the coast to 26 km further inland.

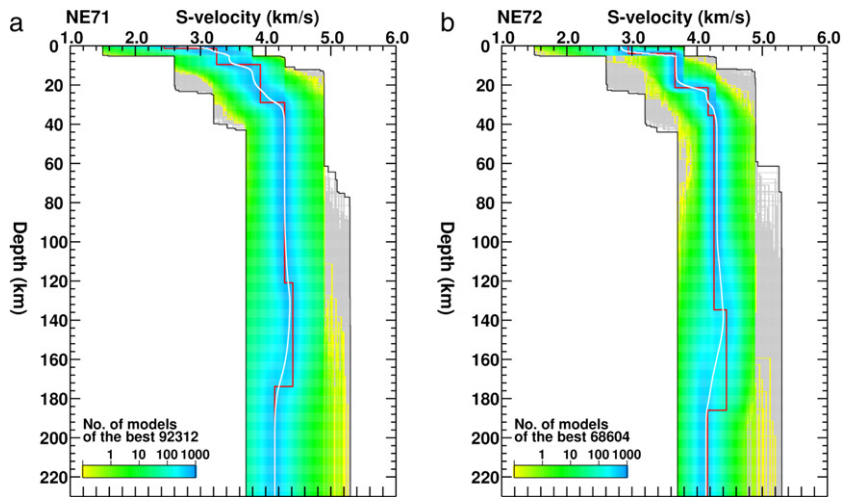


Fig. 7. Model distributions for the joint inversions for station (a) NE71, and (b) NE72. See Fig. 4 caption for further explanation.

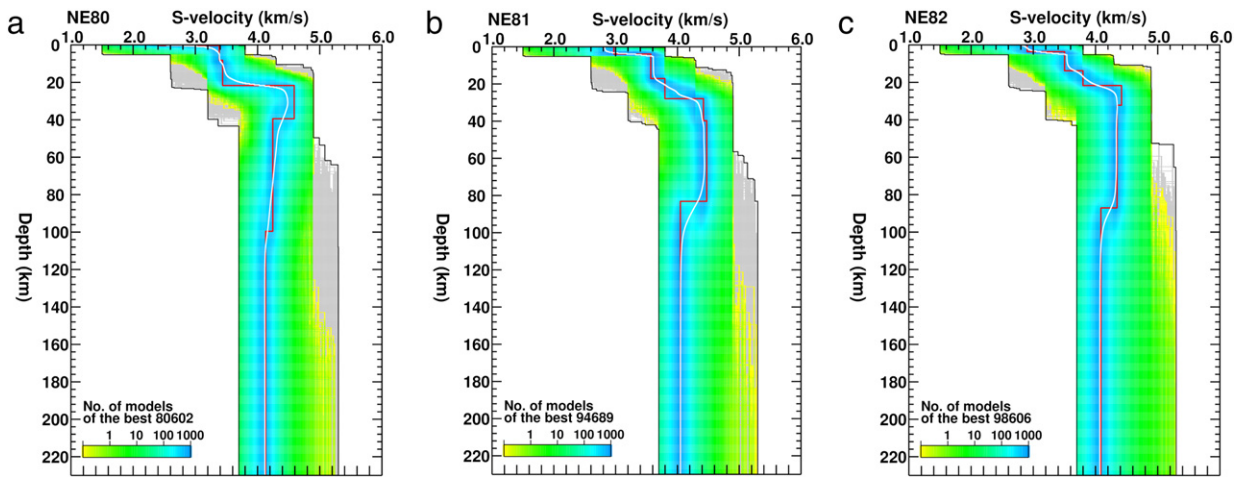


Fig. 8. Model distributions for the joint inversions for station (a) NE80, (b) NE81, and (c) NE82. See Fig. 4 caption for further explanation.

Our results of crustal thinning towards the gulf are in agreement with previous studies using wide-angle data (Lizarralde et al., 2007) and receiver functions (Persaud et al., 2007). Our study improves upon this last study in the amount of data used (two vs. six years of NARS-Baja data) as well as on the inversion technique. Persaud et al. (2007) used the method of Zhu and Kanamori (2000) in which the crust is modelled as a single layer with crustal thickness (H) and V_p/V_s ratio (κ) as inversion parameters. We find that our Moho depths generally are a few km shallower than their results. This is explained in a recent study of Yeck et al. (2013) that showed that the $H - \kappa$ method overestimates the crustal thickness by an amount roughly equal to the sediment thickness. Furthermore, for station NE80 there is a notable discrepancy between the Moho estimates of Persaud et al. (2007) (31–33 km) and ours (20–22 km). Our results are probably more reliable because they are in good agreement with the seismic reflection and refraction studies by González-Fernández et al. (2005) and Lizarralde et al. (2007). These studies find Moho depths of approximately 20 km in the vicinity of station NE80.

Although we only interpreted the most robust features of our crustal models and obtained reasonable estimates of sediment thickness and Moho depth, one might question how reliable the 1-D inversions are, given the back-azimuthal variability of the receiver functions. We therefore modelled the back-azimuthal dependence of the receiver functions of station NE71, the station with the largest back-azimuthal Moho depth variations, by a crustal model with dipping layers. The presentation of the analysis and the results are beyond the scope of this paper and can be found in de Vos (2016). The study showed that most of the back-azimuthal variations that are observed on the radial and transverse receiver functions of NE71 can be explained by a northeasterly dipping mid-crustal interface and a Moho at 28 km depth that dips roughly 30° to the West.

Table 2
Sediment thickness and Moho depth ranges obtained from receiver function inversions for SE, SW and NW back azimuths as well as for all receiver functions together.

Station	Sediment thickness (km)	Moho depth (km)
NE71	0–2	25–32
NE72	2–5	29–32
NE73	1–2	34–38
NE75	1–2	26–27
NE76	2–5	20–22
NE77	1–4	22–26
NE79	0–5	19–24
NE80	1–2	20–22
NE81	0–1	24–26
NE82	2–4	22–24

4. Implications of upper mantle structure

The most striking feature of the upper mantle models is the high-velocity layer with a sharp velocity increase at the top for stations NE73 to NE79 located on the Baja California peninsula. Multiple studies have suggested that slab remnants of the Guadalupe and Magdalena microplates should be present beneath the peninsula (e.g., Calmus et al., 2011; Schellart et al., 2010; Stock and Hodges, 1989), and previous surface wave studies have interpreted high-velocity anomalies as slab signature (Di Luccio et al., 2014; Wang et al., 2013; Zhang and Paulssen, 2012). However, the depth extent of these high-velocity anomalies varied substantially between these studies, ranging from less than 100 km (Di Luccio et al., 2014) to more than 150 km (Wang et al., 2013; Zhang and Paulssen, 2012). The low-misfit models of our study show a remarkable consistency for the top of the high-velocity anomaly with depths around 120–130 km. This suggests that the Guadalupe and Magdalena slab fragments are located at similar depths beneath the Baja California peninsula. The sharpness of the velocity increase at the top of the anomaly, as inferred from the receiver function inversions, can be attributed to the compositional change at the slab interface. The bottom of the high-velocity anomaly shows a greater variability with depths from about 150 km (NE75) to 170 km (NE79) and 190 km (NE73, NE76 and NE77). These depths are more poorly constrained but could indicate variations in slab thickness. A quick estimate of the slab dip can be determined from the slab depth and distance to the former trench. Assuming a constant dip, a slab interface at 130 km and a distance of 275 km between trench and station, a slab dip of 25° is obtained. Although this is only a crude estimate, such a small slope is not unrealistic considering the young age of the subducted Guadalupe and Magdalena slab fragments.

The lateral extent of the subducted slab segments was also unclear from previous studies. Where Zhang et al. (2009) and Zhang and Paulssen (2012) found indications for a slab fragment below the Gulf of California, it is more clearly identified beneath the central part of the Baja California peninsula by Wang et al. (2013). Moreover, Di Luccio et al. (2014) found an additional high-velocity anomaly below the southern part of the peninsula. Although we do not sample the two large regions between stations NE73 and NE75, and NE77 and NE79, we find evidence for a slab signature for all the six stations on the peninsula from NE73 to NE79.

The absence of the high-velocity layer in the model distributions for stations NE71 and NE72 suggests that there is no slab beneath these stations. Indeed, a slab window beneath the northern part of the Baja California peninsula was proposed by Atwater (1989), but,

except for a strong low-velocity signature beneath the northern part of gulf, previous seismic studies did not constrain its lateral extent very well. Our data indicate that the slab window is limited to the region between stations NE71 and NE72 in the northern part of the peninsula.

Our interpretation of a slab beneath stations NE73 to NE79 and its absence beneath NE71 and NE72 has important implications for the interpretation of observed relative plate motions. GPS measurements presented by Plattner et al. (2007) show that, relative to North America, the Baja California peninsula moves in the same northward direction as the Pacific plate but at a slightly lower rate. An observation that is not well understood is that the motion of Baja California varies along the length of the peninsula. The relative motion between the southern part of the peninsula (between 23°N and 25.6°N, i.e. at latitudes between NE77 and NE79) and the Pacific plate was found to be smaller (3.7 mm/year) than the relative motion between the northern part of the peninsula (between 31°N and 31.5°N, i.e. at latitudes between NE71 and NE72) and the Pacific plate (6.2 mm/year). This implies that the relative motion between the southern part of the peninsula and the North-American plate is larger than the relative motion between the northern part of the peninsula and the North-American plate. Plattner et al. (2009) suggested that the northward migration of Baja California is hindered by its collision with the Sierra Nevada block in the North. Rather than an increased resistance of Baja California with the North-American plate towards the North, we favour stronger coupling between the peninsula and the Pacific in the South. We suggest that the stalled Guadalupe and Magdalena slab fragments beneath the central and southern part of the peninsula produce a strong coupling between the Pacific plate and Baja California. The absence of a subducted slab in the slab window region between stations NE71 and NE72, on the other hand, reduces the coupling between the two, which explains the larger relative motion.

Another implication of our study is related to tearing or detachment of the slab fragments. Several studies have suggested that the cessation of subduction of the Guadalupe and Magdalena microplates is related to slab detachment that occurred either below the Baja California peninsula (e.g., Calmus et al., 2011; Michaud et al., 2006; Pallares et al., 2007), or further to the East beneath the Gulf of California (Castillo, 2008; Ferrari, 2004). The main argument for a slab tear beneath the peninsula is the presence of post-subduction magma types such as adakites and niobium-enriched basalts. These are explained by slab melting along the edges of a slab tear beneath the peninsula caused by upwelling of hot Pacific asthenosphere through the slab tear (Calmus et al., 2011). However, an alternative explanation was presented by Castillo (2008), who suggested that the influx of Pacific asthenosphere beneath the gulf caused partial melting of the hydrous mantle wedge beneath the peninsula. Since we find evidence for the presence of high-velocity slab material beneath most of the NARS-Baja stations on the central and southern part of the Baja California peninsula, a slab tear beneath the peninsula is unlikely. We therefore prefer the interpretation of Castillo (2008).

Lastly, the models for stations located on the Mexican mainland show a layer of higher velocities in the uppermost mantle above a low-velocity upper mantle. The velocity decrease is found around 40 km depth for NE80 and around 80 km for stations NE81 and NE82. The low shallow mantle velocities beneath station NE80 are in agreement with the studies of Wang et al. (2009) and Zhang and Paulssen (2012) that suggested local upwelling and partial melting in the region. The velocity decrease around 80 km depth beneath stations NE81 and NE82, on the other hand, can be associated to the lithosphere-asthenosphere boundary that is globally detected at roughly 100 km (Kind et al., 2012; Rychert and Shearer, 2009) and in the western U.S. at depths of 70–80 km (Kumar et al., 2012). Although the nature of this seismic boundary is not yet fully understood, it is likely that it involves a transition from a dry lithosphere to a hydrous asthenosphere, potentially

with an additional melt fraction (Schmerr, 2012). A hydrous asthenosphere with some melt is likely in this region of (former) subduction due to slab dehydration.

5. Conclusions

We performed 1-D joint inversions based on phase velocity data and receiver functions for stations of the NARS-Baja project to better constrain the upper 200 km of the shear velocity structure beneath the Gulf of California region. Phase velocity data from Zhang and Paulssen (2012) were combined with newly measured receiver functions to determine the most robust features beneath the stations using model searches based on the Neighbourhood Algorithm.

The most important finding of our study is that the models for stations located in central and southern Baja California show a high-velocity anomaly of 40 to 60 km thickness with a sharp velocity increase at the top. These high-velocity anomalies are interpreted as remnants of the subducted Magdalena and Guadalupe microplates with their top slab interface at depths of 115 to 135 km. The absence of the high-velocity anomaly beneath the two stations in the northern part of the peninsula is explained by the presence of a slab window. Our results correlate with GPS data of relative motion between the Baja California peninsula and the Pacific plate. The small relative motion in the South can be attributed by strong coupling produced by the stalled slab remnants beneath the peninsula. The slab window in the North allows larger relative motion.

The mantle structure beneath the Mexican mainland is distinct from that beneath the peninsula, showing a velocity decrease at a depth of 40 km in the North and a decrease around 80 km for two more southern locations. The shallow low-velocity structure in the North can be explained by upwelling beneath the northern part of the gulf. The velocity decrease around 80 km is interpreted as the lithosphere-asthenosphere boundary.

The base of the sediment layer and the Moho are found to be the largest and most consistently determined structural contrasts of the crust. The largest sediment thicknesses were obtained for stations in coastal regions. The largest Moho depths, with values of more than 30 km, are found beneath and west of the Peninsular Ranges. The crustal thickness decreases rapidly to about 20 km at the border of the Gulf of California, both from the Baja California peninsula side as well as from the Mexican mainland. Our Moho depth estimates are smaller and likely less biased than those of Persaud et al. (2007), because our inversions include the effects of a low-velocity sedimentary layer.

Acknowledgments

We thank the people that enabled the NARS-Baja project: Raul Castro and Arturo Pérez-Verti from CICESE, Robert Clayton from Caltech, and Jeannot Trampert and Arie van Wettum from Utrecht University. We thank the authors of the programs of the Neighbourhood Algorithm and Generic Mapping Tools (GMT) that were used in this study. Two anonymous reviewers are thanked for their suggestions that helped to improve the manuscript. This study was financed by The Netherlands Research Centre for Integrated Solid Earth Sciences (ISES), project number 2010-57. The NARS-Baja project was funded by Utrecht University, the Netherlands Organisation for Scientific Research (NWO-GOA-750.396.01) and the US National Science Foundation (EAR-0111650).

References

- Ammon, C.J., Randall, G.E., Zandt, G., 1990. On the nonuniqueness of receiver function inversions. *J. Geophys. Res.* 95, 15303–15318.
- Atwater, T., Winterer, E.L., Decker, R.W., Hussong, D.M., 1989. Plate tectonic history of the northeast Pacific and western North America. *The Eastern Pacific Ocean and Hawaii*. N. The Geology of North America., pp. 499–521.

- Brocher, T.M., 2005. Empirical relations between elastic wavespeeds and density in the Earth's crust. *Bull. Seismol. Soc. Am.* 95, 2081–2092.
- Calmus, T., Pallares, C., Maury, R.C., Aguilón-Robles, A., Bellon, H., Benoit, M., Michaud, F., 2011. Volcanic markers of the post-subduction evolution of Baja California and Sonora, Mexico: slab tearing versus lithospheric rupture of the Gulf of California. *Pure Appl. Geophys.* 168, 1303–1330.
- Calò, M., Bodin, T., Romanowicz, R., 2016. Layered structure in the upper mantle across North America from slab inversion of long and short period seismic data. *Earth Planet. Sci. Lett.* 449, 164–175.
- Castillo, P.R., 2008. Origin of the adakite-high-Nb basalt association and its implications for postsubduction magmatism in Baja California Mexico. *Geol. Soc. Am. Bull.* 120, 451–462.
- de Vos, D., 2016. The crustal and upper mantle structure around the Gulf of California, inferred from surface wave data and receiver functions. PhD thesis Utrecht University. Utrecht Stud. Earth Sci. 108, 125.
- Dickinson, W.R., 1997. Tectonic implications of Cenozoic volcanism in coastal California. *Geol. Soc. Am. Bull.* 109, 936–954.
- Di Luccio, F., Persaud, P., Clayton, R.W., 2014. Seismic structure beneath the Gulf of California: a contribution from group velocity measurements. *Geophys. J. Int.* 199, 1861–1877. <http://dx.doi.org/10.1093/gji/ggu338>.
- Ferrari, L., 2004. Slab detachment control on mafic volcanic pulse and mantle heterogeneity in central Mexico. *Geology* 32, 77–80.
- Fletcher, J.M., Grove, M., Kimbrough, D., Lovera, O., Gehrels, G.E., 2007. Ridge-trench interactions and the Neogene tectonic evolution of the Magdalena shelf and southern Gulf of California: insights from detrital zircon U-Pb ages from the Magdalena fan and adjacent areas. *GSA Bulletin* 119, 1313–1336.
- González-Fernández, A., Da nobeitia, J.J., Delgado-Argote, L.A., Michaud, F., Córdoba, D., Bartolomé, R., 2005. Mode of extension and rifting history of upper Tiburón and upper Delfín basins, northern Gulf of California. *J. Geophys. Res.* 110, B01313. <http://dx.doi.org/10.1029/2003JB002941>.
- Julià, J., Ammon, C.J., Herrmann, R.B., Correig, A.M., 2000. Joint inversion of receiver function and surface wave dispersion observations. *Geophys. J. Int.* 143, 99–112.
- Kind, R., Yuan, X., Kumar, P., 2012. Seismic receiver functions and the lithosphere-asthenosphere boundary. *Tectonophysics* 536–537, 25–43.
- Kind, R., Kumar, P., Yuan, X., Mechie, J., 2012. The lithosphere-asthenosphere boundary observed with USarray receiver functions. *Solid Earth* 3, 149–159. <http://dx.doi.org/10.5194/se-3-149-2012>.
- Langston, C.A., 1979. Structure under mount rainier, washington, inferred from teleseismic body waves. *J. Geophys. Res.* 84 (B9), 4749–4762.
- Lebedev, S., Adam, J.M.-C., Meier, T., 2013. Mapping the Moho with seismic surface waves: a review, resolution analysis, and recommended inversion strategies. *Tectonophysics* 609, 377–394.
- Lewis, J.L., Day, S.M., Magistrale, H., Castro, R.R., Astiz, L., Rebolgar, C., Eakins, J., Vernon, F.L., Brune, J.N., 2001. Crustal thickness of the Peninsular Ranges and Gulf Extensional Province in the Californias. *J. Geophys. Res.* 106 (B7), 13599–13611.
- Lizarralde, D., Axen, G.J., Brown, H.E., Fletcher, J.M., González-Fernández, A., Harding, A.J., Holbrook, W.S., Kent, G.M., Paramo, P., Suther, F., Umhoefer, P.J., 2007. Variation in styles of rifting in the Gulf of California. *Nature* 448, 466–469.
- Lonsdale, P., 1991. Structural patterns of the Pacific floor offshore of peninsular California. In: Dauphin, J.P., Simoneit, B.R.T. (Eds.), *The gulf and 522 peninsular province of the California, AAPG Memoir* 47. pp. 87–125.
- McCrorey, P.A., Wilson, D.A., Stanley, R.G., 2009. Continuing evolution of the Pacific-Juan de Fuca-North America slab window system - a trench-ridge-transform example from the Pacific Rim. *Tectonophysics* 464, 30–42.
- Michaud, F., Royer, J.Y., Bourgois, J., Dymet, J., Calmus, T., Bandy, W., Sosson, M., Mortera-Gutiérrez, C., Sichler, B., Rebolledo-Viera, M., Pontoise, B., 2006. Oceanic-ridge subduction vs. slab break off: plate tectonic evolution along the Baja California Sur continental margin since 15 Ma. *Geology* 34, 13–16.
- Obrebski, M., Castro, R.R., 2008. Seismic anisotropy in northern and central Gulf of California region, Mexico, from teleseismic receiver functions and new evidence of possible plate capture. *J. Geophys. Res.* 113, B03301. <http://dx.doi.org/10.1029/2007JB005156>.
- Özalaybey, S., Savage, M.K., Sheehan, A.F., Louie, J.N., Brune, J.N., 1997. Shear-wave velocity structure in the northern basin and range province from the combined analysis of receiver functions and surface waves. *Bull. Seism. Soc. Am.* 87 (1), 183–199.
- Pallares, C., Maury, R.C., Bellon, H., Royer, J.-Y., Calmus, T., Aguilón-Robles, A., Cotten, J., Benoit, M., Michaud, F., Bourgois, J., 2007. Slab-tearing following ridge-trench collision: evidence from Miocene volcanism in Baja California, México. *J. Volcan. Geotherm. Res.* 161, 95–117.
- Paulssen, H., Visser, J., Nolet, G., 1993. The crustal structure from teleseismic P-wave coda - I. Method. *Geophys. J. Int.* 112, 15–25.
- Persaud, P., Pérez-Campos, X., Clayton, R.W., 2007. Crustal thickness variations in the margins of the Gulf of California from receiver functions. *Geophys. J. Int.* 170, 669–687. <http://dx.doi.org/10.1111/j.1365-246X.2007.03412.x>.
- Plattner, C., Malservisi, R., Dixon, T.H., LaFemina, P., Sella, G.F., Fletcher, J., Suarez-Vidal, F., 2007. New constraints on relative motion between the Pacific plate and Baja California microplate (Mexico) from GPS measurements. *Geophys. J. Int.* 170, 1373–1380. <http://dx.doi.org/10.1111/j.1365-246X.2007.03494.x>.
- Plattner, C., Malservisi, R., Govers, R., 2009. On the plate boundary forces that drive and resist Baja California motion. *Geology* 37, 359–362. <http://dx.doi.org/10.1130/G25360A.1>.
- Rychert, C.A., Shearer, P.M., 2009. A global view of the lithosphere-asthenosphere boundary. *Science* 324, 495–498.
- Sambridge, M., 1999a. Geophysical inversion with a neighbourhood algorithm-I. Searching a parameter space. *Geophys. J. Int.* 138, 479–494.
- Sambridge, M., 1999b. Geophysical inversion with a neighbourhood algorithm-II. Appraising the ensemble. *Geophys. J. Int.* 138, 727–746.
- Sato, Y., 1955. Analysis of dispersed surface waves by means of Fourier Transform I. *Bull. Earthquake Res. Tokyo Univ.* 33, 33–47.
- Schellart, W.P., Stegman, D.R., Farrington, R.J., Freeman, J., Moresi, L., 2010. Cenozoic tectonics of western North America controlled by evolving width of Farallon slab. *Science* 329, 316–319.
- Schmerr, N., 2012. The Gutenberg discontinuity: melt at the lithosphere-asthenosphere boundary. *Science* 335, 1480–1483.
- Shen, W., Ritzwoller, M.H., Schulte-Pelkum, V., 2013b. A 3-D model of the crust and uppermost mantle beneath the Central and Western US by joint inversion of receiver functions and surface wave dispersion. *J. Geophys. Res.* 118, 262–276. <http://dx.doi.org/10.1029/2012JB009602>.
- Shepard, D., 1968. A two-dimensional interpolation function for irregularly spaced data. *Proc. ACM Nat. Confe.* 517–524. <http://dx.doi.org/10.1145/800186.810616>.
- Stock, J.M., Hodges, K.V., 1989. Pre-pliocene extension around the Gulf of California and the transfer of Baja California to the Pacific Plate. *Tectonics* 8 (1), 99–115.
- Trampert, J., Paulssen, H., van Wettum, A., Ritsema, J., Clayton, R., Castro, R., Rebolgar, C., Perez-Vertti, A., 2003. New array monitors seismic activity near the Gulf of California in Mexico. *Eos Trans. AGU* 84 (4), 29–32.
- van der Lee, S., Nolet, G., 1997. Seismic image of the subducted trailing fragments of the Farallon plate. *Nature* 386, 266–269.
- Wang, Y., Forsyth, D.W., Savage, B., 2009. Convective upwelling in the mantle beneath the Gulf of California. *Nature* 462, 449–502.
- Wang, Y., Forsyth, D.W., Rau, C.J., Carriero, N., Schmandt, B., Gaherty, J.B., Savage, B., 2013. Fossil slabs attached to unsubducted fragments of the Farallon plate. *Proc. Natl. Acad. Sci. USA* 110 (14), 5342–5346. <http://dx.doi.org/10.1073/pnas.1214880110>.
- Yeck, W., Sheehan, A.F., Schulte-Pelkum, V., 2013. Sequential H- κ stacking to obtain accurate crustal thicknesses beneath sedimentary basins. *Bull. Seis. Soc. Am.* 103, 2142–2150.
- Zhang, X., Paulssen, H., Lebedev, S., Meier, T., 2009. 3D shear velocity structure beneath the Gulf of California from Rayleigh wave dispersion. *Earth Planet. Sci. Lett.* 279, 255–262. <http://dx.doi.org/10.1016/j.epsl.2009.01.003>.
- Zhang, X., Paulssen, H., 2012. Geodynamics of the Gulf of California from surface wave tomography. *Phys. Earth Planet. Inter.* 192–193, 59–67. <http://dx.doi.org/10.1016/j.pepi.2011.12.001>.
- Zhu, L., Kanamori, H., 2000. Moho depth variation in southern California from teleseismic receiver functions. *J. Geophys. Res.* 105 (B2), 2969–2980.